Dalton Transactions

Cite this: *Dalton Trans.*, 2011, **40**, 4190

www.rsc.org/dalton

PAPER

# Synthesis, characterization, DNA interaction and potential applications of gold nanoparticles functionalized with Acridine Orange fluorophores†

**Tarita Biver,*[a] Nurettin Eltugral,[a] Andrea Pucci,*[a] Giacomo Ruggeri,[a] Alberto Schena,[b] Fernando Secco[a] and Marcella Venturini[a]**

***Received 11th October 2010, Accepted 9th February 2011***
**DOI: 10.1039/c0dt01371d**

Two new water-soluble gold nanoparticles (AO-TEG-Au and AO-PEG-Au NPs) are prepared and characterized. They are stabilized by thioalkylated oligoethylene glycols and functionalized with fluorescent Acridine Orange (AO) derivatives. Despite the different core sizes (11.8 and 3.9 nm respectively) and shell composition, they are both well dispersed and are stable in water, even if some self-aggregation is observed in the case of AO-TEG-Au NPs. However, AO-PEG-Au NPs show much lower emission efficiency with respect to AO-TEG-Au NPs. Spectrophotometric and spectrofluorometric experiments indicate that both types of nanoparticle are able to bind to calf thymus DNA, either by external binding or partial intercalation. Preliminary FACS flow cytometry tests seem to indicate that the AO-TEG-Au nanoparticle is able to cross the cell membrane where it is absorbed by Chinese hamster ovary (CHO) cells at the picomolar concentration level.



## 1. Introduction

Nano-sized metal particles show unique properties and growing applications[1–4] and several examples of the application of gold nanoparticles (Au NPs) have been reported.[5–7] Functional groups on the coating shell can modify the Au NPs properties, *e.g.* modulating their solubility[8] and self-assembly[9] or allowing selective interactions.[10] Different chromophores have been coupled to the Au NPs for the design of sensors[11] and as vehicles for tracers and drugs.[12] In recent years, Au NPs interacting with DNA have been extensively studied for potential applications as, for example, smart bio-based nanoparticle assemblies,[9] new intercalating agents[13] or gene delivery vectors.[3] Rotello and co-workers used functionalized Au NPs to carry oligonucleotides inside the cell.[5] In that case they used oligonucleotides labelled with appropriate fluorophores to detect and monitor the uptake process. Alternatively, Au NPs, which are highly interacting with nucleic acids and traceable, can be prepared through the functionalization of the stabilizing capping layer with fluorescent moieties having a strong affinity for nucleotides. We have, therefore, synthesized fluorescently labelled gold nanoparticles showing both notable optical fluorescent properties and high cellular permeability.

In the present work two new types of water-soluble Au NPs are prepared and characterized. They are stabilized by thioalkylated oligoethylene glycols and functionalized with two similar fluorescent Acridine Orange (AO) derivatives. The AO dye has been chosen because of its strong affinity to DNA and its intrinsic sensitivity and unambiguous fluorescence response upon interaction with DNA.[14–16] In addition strong gold binding by thiolic groups is effective in preventing ligand leakage. One of the binders uses the lipoic acid functionality, as the dithiolane ring is able to chelate the gold surface with an affinity higher than that of the single thiols.[17,18] The interaction of the nanoparticles with calf thymus DNA is analyzed and a preliminary test is performed to verify the ability of the nanoparticles to cross the cellular membrane in view of possible applications.

## 2. Materials and methods

### 2.1. Materials

The reagents used for the synthesis of Acridine Orange functionalized ligands were 3,6-bis(dimethylamino)acridine hydrochloride ($C_{17}H_{19}N_3 \cdot HCl \cdot xH_2O$, >99% Sigma-Aldrich), lipoic acid ($C_8H_{14}O_2S_2$, >98% Sigma-Aldrich), 6-bromo-1-hexanol ($Br(CH_2)_6OH$, >96% Fluka), *N*,*N*′-dicyclohexylcarbodiimide (DCC, >99% Fluka), 1,6-dibromohexane ($Br(CH_2)_6Br$, >97% Fluka), and thiourea ($NH_2CSNH_2$, >99% Sigma-Aldrich). 1,6-Dibromohexane and toluene (Aldrich) were distilled prior to use. All the other solvents employed in the synthetic processes were reagent grade (Carlo Erba or Aldrich) and used as received.

Calf thymus DNA (DNA, lyophilized sodium salt, highly polymerized – Sigma) was dissolved in water and sonicated in order to reduce its length. DNA samples (*ca.* $2 \times 10^{-3}$ M, 8 mL) were sonicated in a MSE-Sonyprep sonicator by applying

[a]*Department of Chemistry and Industrial Chemistry, University of Pisa, Via Risorgimento, 35-56126, Pisa, Italy. E-mail: tarita@dcci.unipi.it, apucci@ns.dcci.unipi.it; Fax: 39-0502219260*
[b]*Institute of Chemical Science and Engineering, École Polytechnique Fédérale de Lausanne, Station 6, CH-1015, Lausanne*

† Electronic supplementary information (ESI) available. See DOI: 10.1039/c0dt01371d

 

twenty consecutive cycles of 10 s sonication and 20 s pause with an amplitude of 98 μm. The sonicator tip was directly introduced into the solution which was kept in an ice-bath to minimize thermal effects caused by sonication. Agarose gel electrophoresis tests indicated that the polymer length was reduced to *ca.* 800 base pairs. Stock solutions of DNA were standardized spectrophotometrically ($\varepsilon = 13200\ M^{-1}\ cm^{-1}$ at 260 nm, 0.1 M NaCl and pH = 7.0 for a molar DNA concentration, $C_{DNA}$, expressed in base pairs).[19] Sodium chloride or sodium nitrate (Fluka) were used to adjust the ionic strength and 0.01 M sodium cacodylate (NaCac = $(CH_3)_2AsO_2Na$, Fluka) was employed to keep the pH of the solutions at the value of 7.0. The water used to prepare the solutions and as a reaction medium was purified by a Millipore Milli-Q water purification system.

**6-(3′,6′-Bisdimethylaminoacridinium)hexan-1-ol bromide (AHB).** The AO base was prepared by the addition of ammonium hydroxide to a methanol solution of the AO·HCl salt (99%, Sigma-Aldrich) and subsequent AO base extraction with benzene. The organic phases were collected and dried over anhydrous sodium sulfate and concentrated *in vacuo*. The AO base (0.17 g, 0.64 mmol) in 8 mL anhydrous toluene was heated to 80 °C under stirring for 30 min to obtain a homogeneous solution to which 6-bromo-1-hexanol (1.0 g, 5.5 mmol) was added dropwise over 5 min. The orange solution was heated to reflux (110 °C) and after 10 min a bright red precipitate started to form. The suspension was refluxed overnight, and then filtered over a 200 μm Teflon filter. The precipitate was washed with hot toluene and dried *in vacuo* to obtain a bright red crude solid. The crude product was purified by column chromatography on silica gel, eluting with $CH_2Cl_2$–MeOH–AcOH = 95 : 5 : 1 to yield 6-(3′,6′-bisdimethylaminoacridinium)hexan-1-ol bromide (AHB) as a bright red solid (100 mg, 35%).

$^1$H NMR (300 MHz, $CDCl_3$) $\delta$ (ppm): 8.67 (s, 1H), 7.90 (d, 2H, $J$ = 9.29 Hz), 7.03 (dd, 2H, $J$ = 1.48, 9.27 Hz), 6.63 (s, 2H), 4.79 (t, 2H, $J$ = 7.55 Hz), 3.75 (t, 2H, $J$ = 6.37 Hz), 3.33 (s, 12H), range 1–2 (several m, 8H).

**6-(3′,6′-Bisdimethylaminoacridinium)-1-hexyl lipoate bromide (AHLB).** A three-necked round-bottomed flask equipped with a magnetic stirrer, a reflux condenser and a pressure equalizing dropping funnel were loaded with 6-(3′,6′-bisdimethylaminoacridinium)hexan-1-ol bromide (AHB, 100 mg, 0.22 mmol), dimethylaminopyridine (DMAP, 25 mg, 0.21 mmol) and lipoic acid (100 mg, 0.49 mmol) dissolved in 6 ml of anhydrous dichloromethane. The mixture was stirred and, after complete dissolution of the solid, the flask was cooled in an ice-water bath. *N*,*N*′-Dicyclohexylcarbodiimide (DCC, 150 mg, 0.73 mmol) dissolved in 2 mL of anhydrous dichloromethane was added dropwise to the cooled solution over 10 min. The solution was then allowed to reach room temperature and, after 10 min, a white solid precipitated. The mixture was stirred at room temperature overnight (the temperature was maintained below 40 °C to prevent polymerization of the lipoic acid derivative). The precipitate was filtered with a 200 μm Teflon filter and then washed with dichloromethane (the lipoic acid derivative was dissolved in dichloromethane to prevent polymerization). The organic phase was washed first with 0.5 M HCl, followed by saturated sodium bicarbonate solution and brine. After the extraction, the organic phase was filtered to remove solid impurities and dried over anhydrous sodium sulfate. The product was purified by column chromatography on silica gel, eluting with MeOH–$CHCl_3$ mixture (0 to 5%) to obtain the product as a bright orange oil (15 mg, 10.5%).

$^1$H NMR (300 MHz, $CDCl_3$) $\delta$ (ppm): 8.69 (s, 1H), 7.90 (d, 2H, $J$ = 9.29 Hz), 7.03 (dd, 2H, $J$ = 1.48, 9.27 Hz), 6.55 (s, 2H), 4.73 (t, 2H, $J$ = 7.55 Hz), 4.04 (t, 2H, $J$ = 6.37 Hz), 3.51 (m, 1H), 3.29 (s, 12H), 3.07 (m, 2H), 2.40 (m, 1H), 2.27 (t, 2H, $J$ = 7.18 Hz), range 1–2 (several m, 15H). $^{13}$C NMR (300 MHz, $CDCl_3$) $\delta$ (ppm): 173.7, 155.7, 143.5, 142.7, 133.6, 177.2, 114.2, 92.7, 64.2, 56.5, 47.8, 41.0, 40.3, 38.6, 34.6, 34.1, 28.8, 28.6, 26.9, 26.3, 26.0, 24.7.

**AO-TEG-Au nanoparticles.** A solution of tetrachloroauric acid ($HAuCl_4 \cdot 3H_2O$, Sigma; 37 mg, 0.094 mmol) dissolved in isopropanol (40 mL) was added to a 100 mL Erlenmeyer flask, equipped with a magnetic stirrer. A solution of monohydroxy-(1′-mercaptoundec-11-yl)tetraethylene glycol (12 mg, 0.033 mmol) dissolved in isopropanol (2 mL) and a solution of AHLB acridinium ligand (7.5 mg, 0.012 mmol) also in isopropanol (1 mL) were added. A freshly prepared solution of sodium borohydride (117 mg, 3.1 mmol) in methanol (5 mL) was added dropwise over 1 min. The cloudy suspension became dark green–brown and was left to react at room temperature for 4.5 h. The suspension was poured into n-hexane (200 mL) and a dark brown precipitate formed, that was cooled at −20 °C overnight. The supernatant hexane was removed by centrifugation and the precipitate was washed with diethyl ether and ethyl acetate. The precipitate turned black and was dissolved in a few millilitres of water. The suspension was then dialyzed through a membrane (Spectra/por Floatalyzer MWCO = 3500) under continuous stirring at room temperature for 20 days (deionized water in the flask was changed daily). The disappearance of the free ligand was monitored by UV-vis spectrophotometry. The dialyzed nanoparticle solution in water was assumed to be the stock solution to be employed in subsequent measurements. A schematic drawing of the obtained nanoparticle (AO-TEG-Au) is shown in Fig. 1A.

**10-(6-Bromohexyl)-3′,6′-bisdimethylaminoacridinium bromide (BAHB).** The AO base (0.41 g, 1.6 mmol) in 40 mL anhydrous toluene was heated to 80 °C under stirring for 30 min to obtain a homogeneous solution. 1,6-Dibromohexane (3.80 g, 16 mmol) was added to give an orange solution that was heated to reflux (110 °C). After 20 min a bright red precipitate formed and the suspension was allowed to reflux overnight. The supernatant toluene was removed by centrifugation and the precipitate was washed with toluene, which was then removed under reduced pressure to give a bright red crude solid. The crude product was purified by column chromatography on silica gel, eluting with $CH_2Cl_2$–MeOH = 7 : 1 to yield 10-(6-bromohexyl)-3,6-bisdimethylaminoacridinium bromide (BAHB) as a bright red solid (0.58 g, 73%).

$^1$H NMR (300 MHz, $CDCl_3$) $\delta$ (ppm): 8.75 (s, 1H), 7.91 (d, 2H, $J$ = 9.20 Hz), 7.00 (dd, 2H, $J$ = 2.20, 9.40 Hz), 6.61 (s, 2H), 4.89 (t, 2H, $J$ = 7.00 Hz), 3.45 (t, 2H, $J$ = 6.60 Hz), 3.31 (s, 12H), 1.6–2.0 (several m, 8H). $^{13}$C NMR (300 MHz, $CDCl_3$) $\delta$ (ppm): 155.6, 143.4, 142.7, 133.5, 177.2, 114.0, 93.0, 48.1, 41.2, 34.4, 32.5, 28.1, 26.3, 26.1.

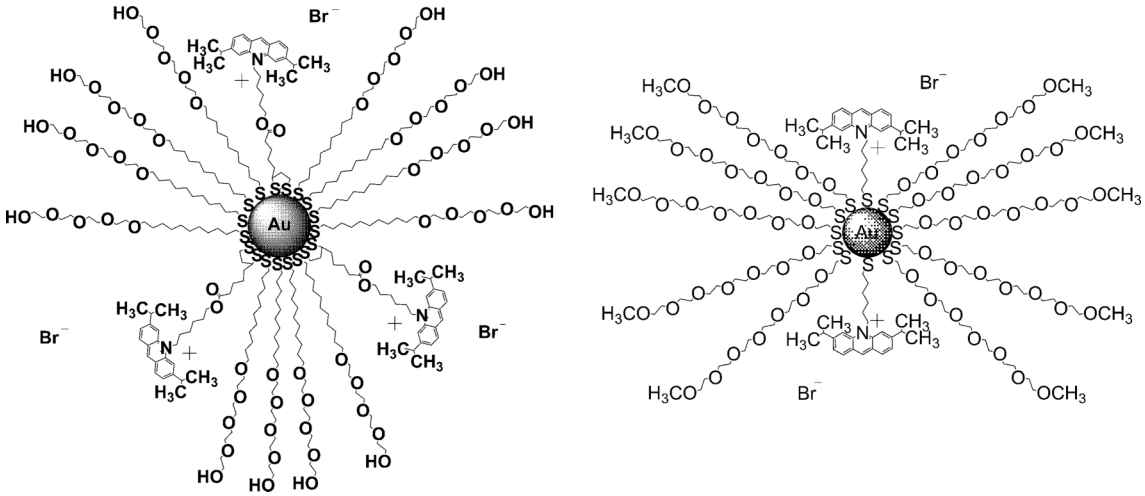


**Fig. 1** Schematic drawing of the AO-TEG-Au and AO-PEG-Au nanoparticles used in the present work.

**Bis(6-(3′,6′-bisdimethylaminoacridinium)hexyl bromide) disulfide (BAHBS).** Thiourea (45 mg, 0.36 mmol) was dissolved in 35 mL dry ethanol under an inert atmosphere. After complete dissolution of thiourea under constant stirring, BAHB (0.25 g, 0.50 mmol) was added to the solution. The resulting mixture was refluxed at 90 °C for 22 h. 15 mL aqueous sodium hydroxide solution (34 mg, 0.85 mmol) was then added and the hydration was carried out for an additional 4 h. The reaction mixture was then poured into 150 mL aqueous HCl solution (pH = 4) and extracted with dichloromethane. The collected organic phase was dried over $Na_2SO_4$ to remove any trace of water. The dichloromethane phase was filtered off and the solvent was evaporated under reduced pressure to obtain a crude oil. The crude product was purified by column chromatography on silica gel, eluting with $CH_2Cl_2$–MeOH = 7 : 1 to yield bis(6-(3′,6′-bisdimethylaminoacridinium)hexyl bromide) disulfide (BAHBS) (0.100 g, 22%).

$^1$H NMR (300 MHz, $CDCl_3$) $\delta$ (ppm): 8.66 (s, 2H), 7.90 (d, 4H, $J$ = 9.30 Hz), 7.13 (d, 4H, $J$ = 9.30 Hz), 6.80 (s, 4H), 4.89 (t, 4H, $J$ = 7.50 Hz), 3.34 (s, 24H), 2.72 (t, 4H, $J$ = 6.90 Hz), 1.6–2.0 ppm (m, 16H). FTIR $\bar{\nu}$/cm$^{-1}$: 2918, 2852, 1640, 1602, 1523, 1503, 1364, 1166, 746, 518.

**AO-PEG-Au nanoparticles.** $HAuCl_4 \cdot 3H_2O$ (35 mg, 0.089 mmol) was dissolved in 50 mL methanol and 0.5 mL glacial acetic acid. Then, a solution of *O*-(2-mercaptoethyl)-*O*′-methylhexa(ethylene glycol) (20 mg, 0.056 mmol) in methanol (2 mL) and a solution of bis(6-(3′,6′-bisdimethylaminoacridinium)hexyl bromide) disulfide (BAHBS) (8.3 mg, 0.009 mmol) also in methanol (4 mL) were added to the gold solution and mixed under constant stirring. A freshly prepared sodium borohydride (112 mg, 3.0 mmol) solution in methanol (5 mL) was added dropwise to the resulting cloudy suspension. The solution immediately turned from orange to dark green–brown, revealing nanoparticle formation. After a further 4 h of stirring, the solution was concentrated under reduced pressure and re-dispersed in isopropanol (50 mL). The particles were precipitated by pouring the mixture into *n*-hexane. The solution mixture was left at –20 °C overnight. The supernatant solution was centrifuged and the collected dark brown precipitate was washed with diethyl ether. The precipitate was then dissolved in 5 mL doubly distilled water and loaded into a dialysis membrane (Spectra/por Floatalyzer MWCO = 3500). The suspension was dialyzed with continuous stirring at room temperature for three days (deionized water in the flask was changed daily). The disappearance of the free ligand was monitored by UV-vis spectrophotometry. The final solution of nanoparticles in water was assigned as the stock and kept at 4 °C. A schematic drawing of the obtained nanoparticle (AO-PEG-Au) is shown in Fig. 1B.

### 2.2. Apparatus and methods

$^1$H- and $^{13}$C NMR spectra were recorded at 20 °C with a Varian Gemini 300 MHz spectrometer using 5–10% analyte concentration in $CDCl_3$. Chemical shifts were assigned in ppm using the solvent signal as a reference. $^1$H NMR was used to evaluate the ligand composition of the prepared gold nanoparticles. In particular, the fraction of the two different ligands that constitute the coating layer was determined by comparing the integrated area of acridine signals (6.5–9 ppm range) to the integrated area of ethylene glycol protons (3.5–4 ppm range). This allows the molar fraction of the acridinium derivative with respect to the total ligand amount to be determined.

Fourier transform infrared (FT-IR) spectroscopy spectra were recorded at room temperature with a Perkin-Elmer Spectrum One spectrometer.

Transmission electron microscopy (TEM) experiments were carried out either in a JEOL-1200 transmission electron microscope using an acceleration voltage of 120 kV or in a Philips CM 200 electron microscope working at 200 kV. Scanning electron microscopy (SEM) experiments were carried out by means of a Field Emission ZEISS SUPRA 40 scanning electron microscope. A single drop (10 µL) of a dilute aqueous solution of Au NPs (*ca.* 0.1 mg mL$^{-1}$) was placed on a copper grid coated with a carbon film. The grid was allowed to dry in a desiccator for several hours at room temperature. Size distributions of the nanoparticle cores were measured from enlarged TEM images for at least 200 individual cluster core images using the Image Tool 3.00 image analyzer software developed at the University of Texas

 

Health Science Center in San Antonio and available online at http://ddsdx.uthscsa.edu/dig/itdesc.html.

X-Ray diffraction (XRD) patterns were obtained in Bragg-Brentano geometry with a Siemens D500 KRISTALLOFLEX 810 (count time per step: 1.0 s; step size: 0.050° and Cu-Kα, $\lambda$ = 1.541 Å) diffractometer. Data were acquired at room temperature.

To evaluate the gold content (mg $L^{-1}$) of the stock nanoparticle solutions, atomic absorption (AA) measurements were made on a Perkin Elmer Analyst 100 spectrophotometer. The stock nanoparticle solution was dried under reduced pressure at 35 °C to constant weight; then the recovered nanoparticles were re-dispersed in precisely known volumes of water. To overcome matrix effects of the nanoparticle solutions, the concentrations were evaluated by the method of standard additions using special grade standards (Aldrich).

Spectrophotometric measurements were carried out on a Perkin Elmer Lambda 35 spectrophotometer, while fluorescence measurements were performed on a Perkin Elmer LS55 spectrofluorometer, both with temperature control to within ± 0.1 °C. The stability of nanoparticles was monitored by UV-visible spectrophotometry, using the surface plasmon resonance band.[20] Absorbance and fluorescence titrations of DNA/nanoparticle systems were done by adding increasing amounts of the polynucleotide directly into the cell containing the nanoparticles solution by means of a syringe connected to a micrometric screw. In the case of the absorbance measurements data have been collected in a differential manner; namely, the same amount of DNA was placed in both the sample and reference cuvettes, to compensate for the DNA contribution to the measured signal in the UV range. AO-TEG-Au and AO-PEG-Au NPs concentrations are expressed in AO molarity and labelled as $C_{AO}$. In this way a direct comparison can be made between binding constants evaluated for the NPs/DNA systems and for the AO derivative/DNA system.

Cellular uptake tests were made by means of fluorescence activated cell sorting (FACS) flow cytometry analysis on Chinese hamster ovary (CHO) immortalized cells. CHO cells were grown in 10 cm plates to confluency in F12 Ham's media (10% FBS and 1× Pen/Strep). After one day the cells were left with 1 mL of trypsin and incubated for 5 min at 37 °C. Then the cells were passaged: 14 well plates (1 for blank, 6 for free ligand, 7 for Au NPs) were prepared with 25 µL of a diluted (1 : 40) tryptinized suspension into 1 mL of media each. After three days the cells were confluent and ready for the FACS analysis. The cellular uptake was evaluated on the functionalized gold nanoparticles. Working solutions of the Au NPs (0.14 to 9.6 nM) were prepared by dilution with phosphate saline buffer (PBS) of a 50 nM stock, to reach the final volume of 1 mL. For treatment of the cells each sample was prepared as follows: the media were removed from the cell plate and the cells were washed with 3× PBS; the washing buffer was removed and the plate was treated with the buffered sample solution. Pure PBS was added to the blank plate. The cells were incubated at 37 °C for 1 h; then the solutions were removed and the cells were washed several times with 5× PBS and 1 mL of 1× trypsin was added. After 10 min incubation at 37 °C the suspension was transferred into FACS tubes and spun down by 10 min centrifugation at 1000 rpm. The supernatant media was removed from the pellets and 500 µL of BSA medium (0.1% Bovine Serum Albumin + 5 mM EDTA in PBS) were added, shaking to re-suspend the cells. Each solution was analyzed with a BD FACS Calibur flow cytometer, subtracting the blank signal of the cells treated with pure PBS buffer. Statistics were performed on 10000 cells. In the FACS apparatus the wavelength of the exciting laser was 480 nm, while the emission intensity was 520 nm. The high sensitivity required for the low concentrations detected in our FACS experiments could be attained due to the fact that the standard excitation wavelength is very close to the absorption maximum of the AHLB ligand, and that the maximum emission intensity of the acridinium moiety almost coincides with the maximum intensity of the detector.

**Table 1** Characteristic parameters of the AO-TEG-Au and AO-PEG-Au nanoparticles synthesized in the present work

| | AO-TEG-Au | AO-PEG-Au |
|---|---|---|
| Average diameter from TEM (nm) | 11.8 ± 3.4 | 3.9 ± 1.0 |
| Av. no. Au in a NP core | $5.1 \times 10^4$ | $1.8 \times 10^3$ |
| Average MW (Da) | $1.2 \times 10^7$ | $5.2 \times 10^5$ |
| Average TEG (PEG)/AO ratio (from $^1$H NMR) | 5 | 16 |
| Av. no. AO in a NP | 700 | 28 |
| Av. no. TEG (PEG) in a NP | $3.7 \times 10^3$ | $4.5 \times 10^2$ |
| Av. no. total stabilizer tails in a NP | $4.4 \times 10^3$ | $4.8 \times 10^2$ |
| Au/total stabilizer ratio in a NP | 12 | 4 |

## 3. Results

### 3.1. Nanoparticles synthesis

In the first synthetic approach (preparation of AO-TEG-Au NPs), the AO was connected to the nanoparticle surface through a linker between the 9 position of the acridine ring and a terminal lipoic acid moiety.[21,23] This functional ligand was used together with the main stabilizing ligand monohydroxy(1-mercaptoundec-11-yl)tetraethylene glycol (TEG-SH). The second approach (preparation of AO-PEG-Au NPs) is based on the use as stabilizing ligand of a mixture of the synthesized AO-hexyl disulfide derivative (BAHBS)[22,23] and *O*-(2-mercaptoethyl)-*O*′-methylhexa(ethylene glycol) (m-PEG-SH). Both TEG-SH and m-PEG-SH provide highly hydrophilic shells.[8] AHLB was prepared following the synthetic procedure described in Scheme 1, whereas BAHBS was synthesized according to Scheme 2.

Au NPs were prepared following a single-phase reduction method in alcoholic solution,[8] as reported in detail above. The disulfide is expected to behave in the same way as the corresponding thiol, since it is well established that the chemisorption of an *n*-alkyl disulfide on a Au NPs surface occurs in a similar manner to that of the corresponding alkanethiol.[24]

### 3.2. Nanoparticles characterization

The dispersity of the particle distribution and their sizes was determined by TEM analysis (Fig. 1S and 2S of ESI† for AO-TEG-Au NPs and AO-PEG-Au NPs, respectively). The nanoparticles were found to be spherical to a good approximation with mean core diameters of 11.8 ± 3.4 nm for AO-TEG-Au NPs and 3.9 ± 1.0 nm for AO-PEG-Au NPs (Table 1). For the AO-PEG-Au nanoparticles SEM and XRD experiments were also performed (Fig. 3S and 4S of ESI†) that yielded a mean nanoparticle diameter of 4.6 ± 0.8 nm (SEM) and 5.8 nm (XRD, on applying Scherrer's equation on the Au(111) peak).[25] The results obtained by the different techniques are in fairly good agreement.

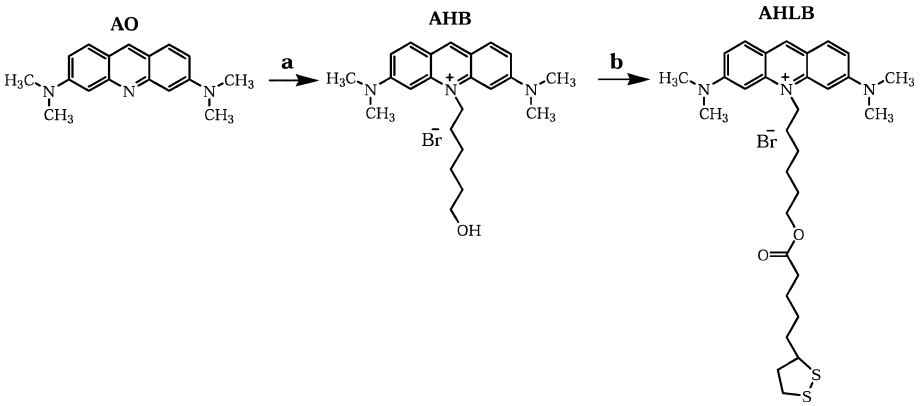


**Scheme 1** Synthesis of acridinium lipoate (AHLB). *Reagents and conditions*: (a) 9 eq. 6-bromo-1-hexanol, toluene, 110 °C, 24 h; (b) 2.2 eq. lipoic acid, 3.3 eq. DCC, 1 eq. DMAP, $CH_2Cl_2$, r.t., 18 h.

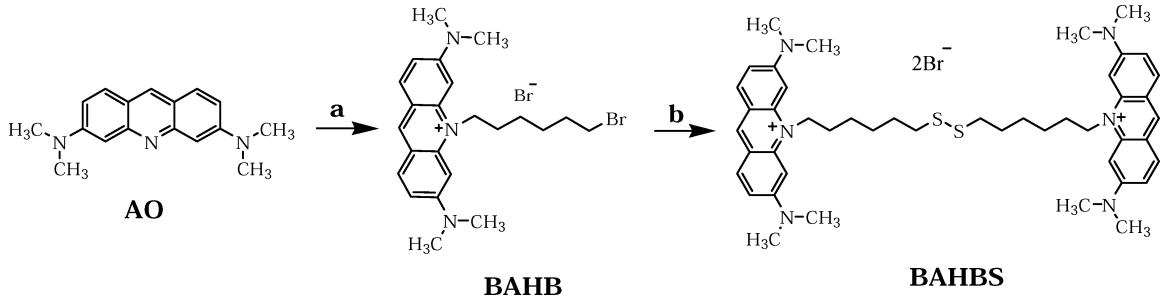


**Scheme 2** Synthesis of bis(6-(3′,6′-bisdimethylaminoacridinium)hexyl bromide) disulfide (BAHBS). *Reagents and conditions*: (a) 10 eq. 1,6-dibromohexane in toluene, reflux at 110 °C, overnight, (b) 0.72 eq. thiourea in ethanol, reflux at 85 °C for 22 h; then 1.7 eq. $NaOH/H_2O$, reflux for 5 h.

The mean number of gold atoms in a particle ($n$) was calculated using eqn (1)[26,27]

$$n = \frac{0.5\pi N_A d_m^{\ 3}}{3V_m} \quad (1)$$

where a spherical particle shape is assumed, $N_A$ is Avogadro's number, $d_m$ is the diameter of the nanoparticle and $V_m$ is the molar volume of gold (10.2 $cm^3$). The gold content (mg $L^{-1}$) and the mixed monolayer composition were determined by the combined use of AA and $^1H$ NMR measurements (see the experimental section and Fig. 5S and 6S of ESI† for AO-TEG-Au NPs and AO-PEG-Au NPs, respectively). These data allowed the average molecular weight and composition of clusters to be estimated (Table 1). The diameter of the AO-TEG-Au NPs with [Au]/[total stabilizer] ratio equal to 12 is about three times larger than the diameter of the AO-PEG-Au NPs with [Au]/[total stabilizer] ratio equal to 4 (Table 1). This behavior is in agreement with similar results reported in the literature for thiol-stabilized Au NPs, which shows that NPs increase significantly their diameter when the [Au]/[total stabilizer] ratio becomes higher than 3.[28]

The Au NPs are found to be well dispersed in water and their stability against both decomposition and/or aggregation was checked using optical spectroscopy. AO-TEG-Au NPs solutions are stable in pure water, but precipitate on addition of salt (0.1 M NaCl or 0.1 M $NaNO_3$). On the other hand, AO-PEG-Au NPs are stable both in pure water and 0.1 M NaCl solutions. Absorbance spectra reveal that both NPs do significantly scatter light (Fig. 7S of ESI†), in agreement with previous findings on similar systems.[29] Therefore, the NPs absorbance data have been corrected for a light scattering (LS) contribution, following the procedure described by Leach and Scheraga that uses double logarithmic plots.[30] One example of spectrum correction is provided in Fig. 8S of ESI†. The two systems display analogous absorption characteristics, with two maxima in the visible region, one centered at around 475 nm independently on the nature of the NPs, and the other at 496 nm for AO-TEG-Au and at 507 nm for AO-PEG-Au NPs (Fig. 2). The presence of two maxima is observed for similar AO derivatives[31] and for AHLB itself (Fig. 9S of ESI†), whereas plasmon bands centered around 500 nm are typical of gold nanoparticles of diameter close to that measured in this work.[29]

As regards the AO-PEG-Au system, the absorption ratio of the two maxima at different NP concentrations is constant, indicating that NPs do not self-aggregate in the investigated concentration range (inset in Fig. 2B). On the other hand, both the AO-TEG-Au NPs and the AHLB molecule undergo some self-aggregation (dimerisation) at higher dye concentrations, as confirmed by the increase of the absorbance ratio $A_{475}/A_{496}$ (insets of Fig. 2A and 9S (ESI†) respectively). The quantitative analysis of the self-aggregation process, described by the simplified dimerisation process shown in reaction (2), can be done by fitting of the data to eqn (3) and (4)

$$2\,M \rightleftharpoons[K_D] D \quad (2)$$

$$A = \varepsilon_M[M] + \varepsilon_D[D] \quad (3)$$

$$C_{AO}/(A - \varepsilon_M C_{AO}) = 2/\Delta\varepsilon + (1/K_D\Delta\varepsilon)(1/[M]) \quad (4)$$

 

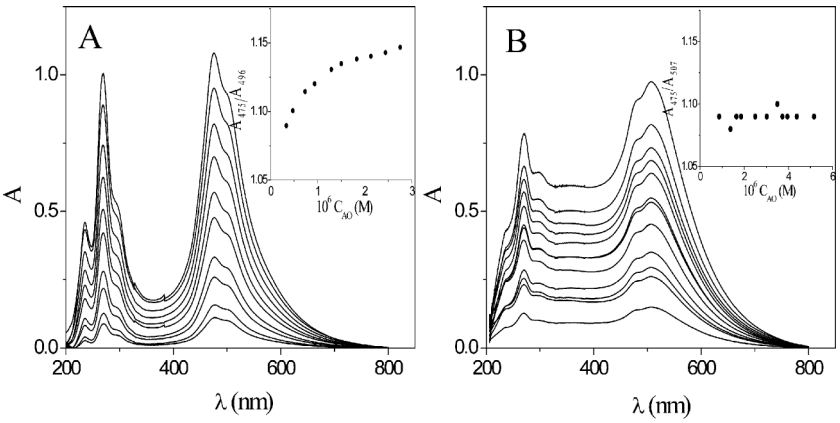


**Fig. 2** Absorbance spectra of AO-TEG-Au NPs (A) and of AO-PEG-Au NPs (B) once corrected for light scattering contribution at various NP concentrations, $T = 25$ °C. (A) $C_{AO} = 3.6 \times 10^{-7}$–$2.9 \times 10^{-6}$ M, pH = 7.0, $I = 0.01$ M (NaCac); (B) $C_{AO} = 3.4 \times 10^{-7}$–$5.2 \times 10^{-6}$ M, pH = 7.0, $I = 0.1$ M (NaCl). The insets are plots of the ratio of the two maxima with respect to NP concentration.

where M is the nanoparticle monomer, D its dimer form, $A$ is the experimental absorbance (corrected for LS in the case of AO-TEG-Au NPs), $\varepsilon_M$ and $\varepsilon_D$ are the molar extinction coefficients of monomer and dimer respectively, $\Delta\varepsilon = \varepsilon_D - 2\varepsilon_M$ and $C_{AO}$ is the total nanoparticle concentration (expressed in AO concentration). For the derivation of eqn (4) see ref. 32. First, a rough estimate of $\varepsilon_M$ was obtained by the spectra and used to plot $C_{AO}/(A - \varepsilon_M C_{AO})$ *vs.* 1/[M] that, in this first estimation, was set equal to $1/C_{AO}$. A linear fit of the data plot according to eqn (4) enabled $K_D$ and $\Delta\varepsilon$ be evaluated. Then, $K_D$ was used to calculate [M] and [D] values for a 3D fit according to eqn (3) that yielded better $\varepsilon_M$ and $\varepsilon_D$ estimates, and the procedure is repeated until convergence is reached. For the AO-TEG-Au NPs it is found that $\varepsilon_M{}^{475\text{ nm}} = (2.80 \pm 0.05) \times 10^5$ M$^{-1}$ cm$^{-1}$, $\varepsilon_D{}^{475\text{ nm}} = (9.47 \pm 0.09) \times 10^5$ M$^{-1}$ cm$^{-1}$ and $K_D = (6.3 \pm 0.3) \times 10^5$ M$^{-1}$; for AHLB $\varepsilon_M{}^{475\text{ nm}} = (2.80 \pm 0.06) \times 10^4$ M$^{-1}$ cm$^{-1}$, $\varepsilon_D{}^{475\text{ nm}} = (1.82 \pm 0.07) \times 10^5$ M$^{-1}$ cm$^{-1}$ and $K_D = (2.7 \pm 0.2) \times 10^3$ M$^{-1}$. The features of the AHLB self-aggregation process here observed are in agreement with those displayed by AO, proflavine and their alkyl-derivated compounds.[16,33,34] The extinction coefficient of AO-PEG-Au NPs in 0.1 M NaCl (Fig. 2B) at 507 nm is $\varepsilon = 4.2 \times 10^5$ M$^{-1}$ cm$^{-1}$ (not corrected for LS) or $\varepsilon = 1.9 \times 10^5$ M$^{-1}$ cm$^{-1}$ (after correction for LS).

### 3.3. DNA interaction

**AO-TEG-Au NPs/DNA.** The binding of AO-TEG-Au NPs to DNA was investigated by spectrophotometric and spectrofluorometric titrations. The interaction is revealed by changes in the absorbance and fluorescence spectra: NP absorbance decreases and fluorescence increases upon addition of increasing amounts of DNA to the NP sample present in the measuring cell (Fig. 3A and 4A). As regards absorbance data, the experimental spectra are shown in Fig. 10S of ESI†, whereas Fig. 3A show the results of the LS correction. The behavior below 300 nm and the binding isotherm at 270 nm (Fig. 3) reveals that the binding process is biphasic, thus suggesting the occurrence of two interaction modes (let's define them as binding mode (1) and binding mode (2)). On the other hand, the isotherm at 475 nm (Fig. 3C) is monophasic and provides information on binding mode (1). Binding mode (2) was investigated by spectrofluorometry (Fig. 4). The maximum emission of the AO-TEG-Au NP/DNA complex (520 nm) is the same as exhibited by the AO/DNA complex,[35] confirming that the acridine moiety is the main DNA binder.

It can be calculated that only 55% of AO-TEG-Au NPs are present as monomer under the conditions of DNA binding experiments; therefore, the interaction between nanoparticles and DNA is expressed by the system of reactions (2), (5) and (6)

$$M + S \leftrightarrows MS \quad (5)$$

$$D + S \leftrightarrows DS \quad (6)$$

where the assumption is made that the nanoparticle could react with a DNA site (S) both in the form of the monomer (M) and in the form of dimer (D), to give the bound species MS and DS respectively. The equilibrium constants of (5) and (6) are defined as $K_{mon} = [MS]/([M][S])$ and $K_{dim} = [DS]/([D][S])$. The titration data were analyzed using eqn (7), that can be obtained on the basis of reactions (2), (5) and (6) (for its derivation see ESI†).

$$\frac{A}{C_{AO}} = \frac{\varepsilon_D}{2} + \frac{\Delta\varepsilon_1 + \Delta\varepsilon_2 K_{mon}[S] + \Delta\varepsilon_3 K_D K_{dim}[M][S]}{1 + 2K_D[M] + K_{mon}[S] + 2K_D K_{dim}[M][S]} \quad (7)$$

where [S] is the free DNA concentration and [M] the free monomer concentration, $\Delta\varepsilon_1 = \varepsilon_M - (\varepsilon_D/2)$, $\Delta\varepsilon_2 = \varepsilon_{MS} - (\varepsilon_D/2)$ and $\Delta\varepsilon_3 = \varepsilon_{DS} - \varepsilon_D$. The 3D data fit to eqn (7) requires an iterative procedure as [S] and [M] have to be calculated using the values of $K_D$, $K_{mon}$ and $K_{dim}$, where $K_D$ only is known. The same procedure was used for fluorescence titrations, by replacing $A$, $\varepsilon_D$ and $\Delta\varepsilon_i$ by $F$, $\varphi_D$ and $\Delta\varphi_i$ respectively. Both analyses evidenced that the $\Delta\varepsilon_3$ ($\Delta\varphi_3$) and $K_{dim}$ contributions can be neglected, indicating NP binds to DNA as a monomer only. Under such circumstances eqn (7) reduces to eqn (8)

$$\frac{A}{C_{AO}} = \frac{\varepsilon_D}{2} + \frac{\Delta\varepsilon_1 + \Delta\varepsilon_2 K_{mon}[S]}{1 + 2K_D[M] + K_{mon}[S]} \quad (8)$$

The obtained values of $K_{mon} = K$ are collected in Table 2. Note that, as the number of Acridine Orange molecules contained in each nanoparticle cluster is known ($n_{AO}$, Table 1), the numerical value of $K$ given in Table 2 can be converted to the binding affinity

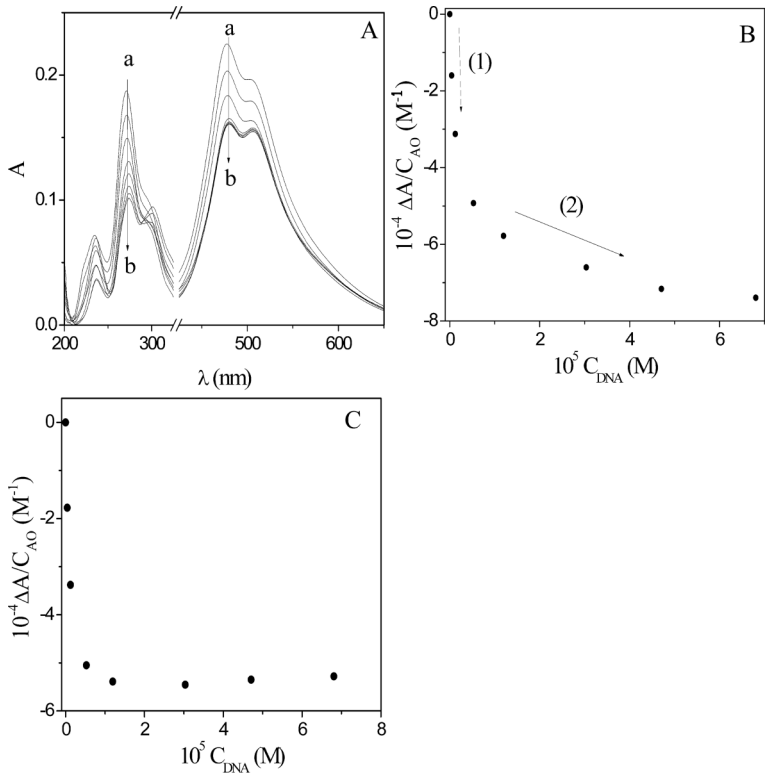


**Fig. 3** (A) Absorbance spectra of the AO-TEG-Au NPs/DNA system (corrected for LS), $C_{AO} = 1.2 \times 10^{-6}$ M, pH = 7.0, $T = 25$ °C, (a) $C_{DNA} = 0$, (b) $C_{DNA} = 6.8 \times 10^{-5}$ M; (B) binding isotherm at 270 nm; (C) binding isotherm at 475 nm.

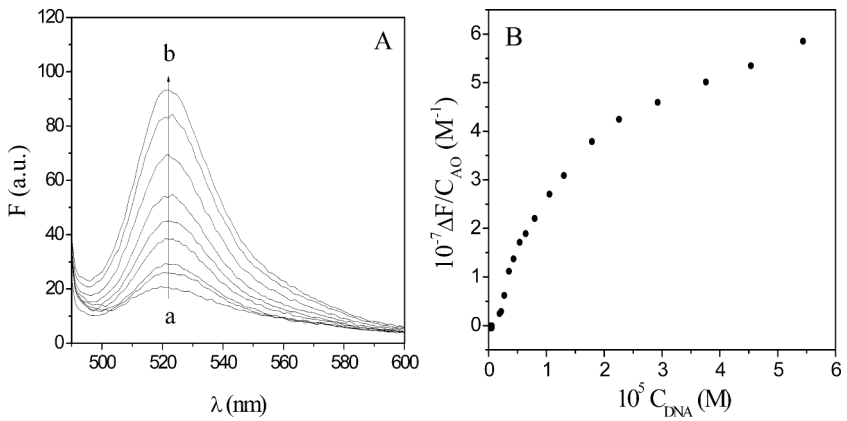


**Fig. 4** (A) Fluorescence spectra collected for AO-TEG-Au NPs/DNA, $C_{AO} = 1.2 \times 10^{-6}$ M; pH = 7.0, $T = 25$ °C. (a) $C_{DNA} = 0$, (b) $C_{DNA} = 6.8 \times 10^{-5}$ M; (B) binding isotherm at $\lambda_{ex} = 480$ nm, $\lambda_{em} = 520$ nm.

of one DNA base pair to one cluster ($K'$) simply by using the relationship $K' = n_{AO}K$.

Control experiments have been done on the interaction with DNA of the free AO derivative (AHLB) in the absence of gold nanoparticles, to be compared with the behavior of the AO-TEG-Au/DNA system. The absorbance spectra of the AHLB/DNA system at different polymer to dye ratios show two different behaviors indicating that two modes of binding are operative (Fig. 5). In particular, upon addition of DNA, an absorbance decrease is first observed till a threshold AHLB/DNA ratio is attained, and then an absorbance recovery occurs with a red-shift of the peak centered at 500 nm.

In the case of the AHLB/DNA system less than 5% dimer is present under conditions of DNA binding experiments and the $K_D$ term in eqn (8) can be neglected; eqn (8), once rearranged, becomes eqn (9).

$$\frac{\Delta A}{C_{AO}} = \frac{K\Delta\varepsilon[S]}{(1+K[S])} \tag{9}$$

where $\Delta A = A - A^0$ and $A^0 = \varepsilon_M C_{AO}$ is the absorbance of the NP solution in the absence of DNA. $\Delta\varepsilon = \varepsilon_{MS} - \varepsilon_M$ is the amplitude of binding isotherm. Initially, the total DNA concentration, $C_{DNA}$, is introduced in eqn (9) in place of [S] to obtain a first estimation of

 

**Table 2** Binding constants to DNA for the two analyzed nanoparticles and for the free AHLB derivative at pH = 7.0, $T = 25\ ^{\circ}C$

| | $K/M^{-1}$ | |
|---|---|---|
| System | Spectrophotometry | Spectrofluorimetry |
| AO-TEG-Au NPs/DNA | $5.4 \times 10^{6\,a}$ ($K_1$) | — |
| | $3.3 \times 10^{4\,b}$ ($K_2$) | $3.8 \times 10^4$ |
| AO-PEG-Au NPs/DNA[c] | $>10^6$ ($K_1$) | — |
| | $<10^5$ ($K_2$) | $2.0 \times 10^4$ |
| AHLB/DNA | $>1.0 \times 10^6$ ($K_1$) | — |
| | $3.5 \times 10^4$ ($K_2$) | $6.3 \times 10^4$ |

[a] Fit to eqn (8) of the data at 475 nm. [b] Fit to eqn (8) of the second part of the data at 270 nm. [c] $I = 0.1$ M (NaCl).

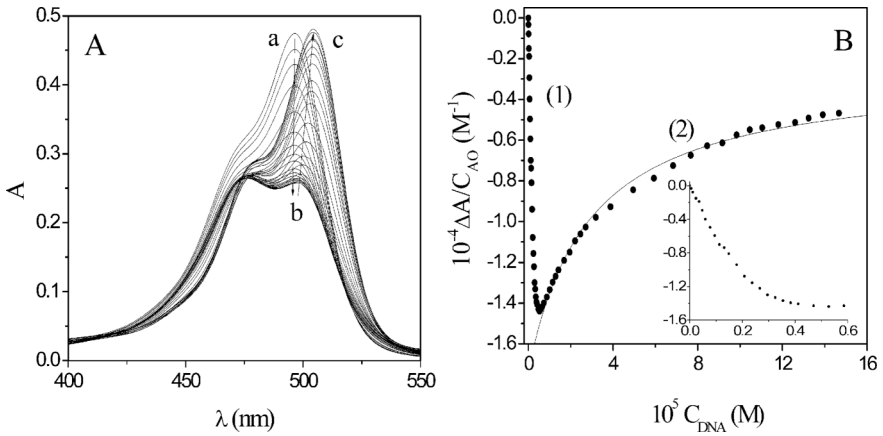


**Fig. 5** (A) Absorbance spectra of the AHLB/DNA system, $C_{AO} = 1.3 \times 10^{-5}$ M, pH = 7.0, $T = 25\ ^{\circ}C$, (a) $C_{DNA} = 0$ M, (b) $C_{DNA} = 5.9 \times 10^{-6}$ M, (c) $C_{DNA} = 1.5 \times 10^{-4}$ M. (B) Corresponding binding isotherm revealing the biphasic behavior of the binding process at 496 nm (the inset is the expansion of the descending portion of the plot). The continuous line represents the trend calculated according to eqn (9).

$K$ that can be used to calculate [MS] and [M] = $C_{DNA}$ − [MS]. Then, $K$ and $\Delta\varepsilon$ are re-evaluated by introducing [M] in eqn (9) and the procedure is repeated until convergence is reached. The two branches of the binding isotherm were analyzed with the help of eqn (9) and the equilibrium constants obtained are shown in Table 2. Fluorescence titrations, done with much more diluted amounts of AHLB ($1.9 \times 10^{-7}$ M) are, on the other hand, monophasic (Fig. 11S of ESI†). The dye fluorescence increases upon DNA addition, as is also observed in the case of the AO/DNA system.[36] The value of $K$, obtained by data fit to eqn (9), is collected in Table 2.

**AO-PEG-Au NPs/DNA.** Several spectroscopic titrations were carried out in 0.1 M NaCl to investigate AO-PEG-Au NPs binding to DNA. The absorbance titration isotherms reveal the presence of two interaction modes (Fig. 12S of ESI†) but the variation of absorbance is too low to enable a quantitative evaluation of the reaction parameters; only lower and upper limits for $K_1$ and $K_2$, respectively, could be estimated (Table 2). The spectrofluorometric method is more sensitive to investigate the binding, but with this technique one binding mode only can be observed (Fig. 13S of ESI†). Fit of the data to eqn (9) yields the binding constants in Table (2). It is worth to emphasize that, differently from AO-TEG-Au NPs, AO-PEG-Au NPs are almost not fluorescent when in solution and it is only when DNA is added that the green–yellowish acridinium fluorescence becomes readily observable.

### 3.4. Cellular uptake tests of the AO-TEG-Au NPs

Preliminary cellular uptake tests were carried out by means of the FACS flow cytometry technique, in order to check if the ability of the AO-TEG-Au NPs to bind nucleic acids could make them suitable for potential applications in biology. It has to be noted that the AO-TEG-Au NPs are self-emissive and, furthermore, the interaction with the nucleic acids can be real-time monitored because of the spectroscopic features widely discussed in the previous sections. A preliminary study was performed on the free ligand AHLB and even at very low concentrations (10 nM AHLB in PBS) saturation conditions were reached; actually, all the Chinese hamster ovary (CHO) cells incubated in the presence of the dye have been shown to incorporate the fluorescent molecule. Then the uptake of the AO-TEG-Au NPs was tested. The FACS analysis was performed on several identical samples of CHO immortalized cells incubated in solutions at variable concentrations of the AO-TEG-Au NPs. The results are shown in Fig. 6. Both the shape of the histograms and the concentration dependence reveal nanoparticle uptake. At $C_{AO}$ = 1.4 nM, a bimodal distribution is observed. A shoulder in the histogram at higher emission intensity appears, relative to the occurrence of the uptake of NPs. Below 1.4 nM the uptake is negligible, as indicated by the strongly reduced level of cell fluorescence. At 2.8 nM almost all the cells have shown to contain the AO-TEG-Au NPs and above 7 nM saturation of the system is reached, such that the maximum number of functionalized nanoparticles has entered living cells

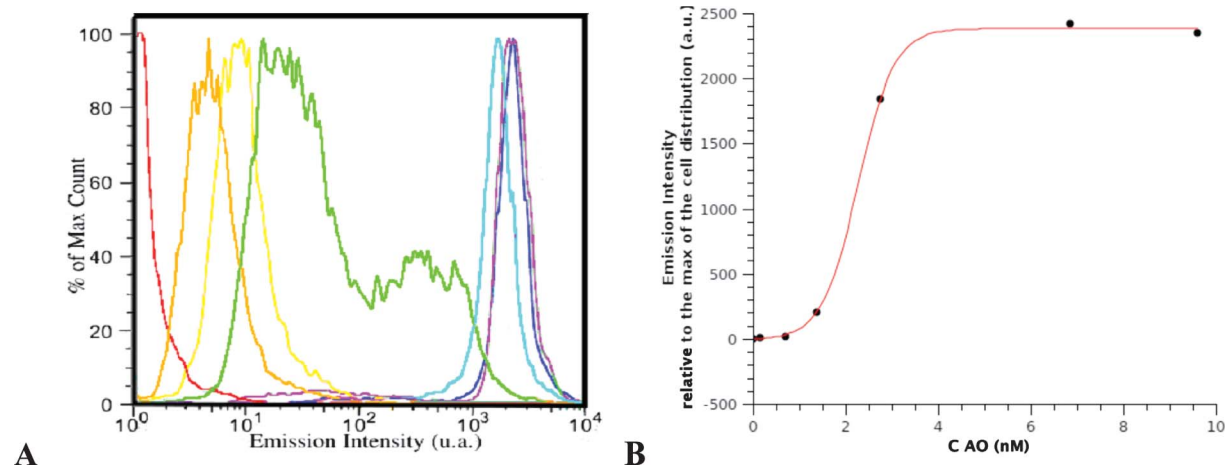


**Fig. 6** (A) Statistical distribution of the FACS data at different nanoparticle concentrations (in AO molarity): cell count *vs.* fluorescence intensity at 520 nm for $C_{AO} = 0$ (red), 0.14 (orange), 0.7 (yellow), 1.4 (green), 2.8 (cyan), 7.0 (blue) and 9.6 (violet) nM. (B) Emission intensity relative to the maximum of the distribution of the cell count *vs.* the AO-TEG-Au NP concentration.

and no significant change is observed if the concentration of the incubation solution is higher.

## 4. Discussion

Acridine orange functionalized water-soluble gold nanoparticles have been successfully synthesized using different ethylene glycol based ligands and acridine derivatives. They have different core sizes (11.8 nm for AO-TEG-Au NPs and 3.9 nm for AO-PEG-Au NPs) and shell composition, but are both stable against precipitation in water over a period of months when kept at +4 °C. AO-PEG-Au NPs are stable also in the presence of added salts (0.1 M NaCl or $NaNO_3$), whereas AO-TEG-Au NPs stability is sensitive to electrolyte concentration (regardless of salt type). As Acridine Orange self-association is promoted when salt is added to aqueous dye solutions, this effect could induce nanoparticle precipitation. In particular, in the case of the AO-TEG-Au NPs, the higher number of AO residues in the shell (700 against 28 for the AO-PEG-Au system) could be the cause of the higher self-aggregation tendency of this (bigger) nanoparticle; the same effect is actually less probable in case of the smaller AO-PEG-Au NPs where, moreover, AO is more buried into the PEG ligand. The above qualitative findings agree with the results of the quantitative analysis of the absorbance features of the two nanoparticles at different NP concentrations. Indeed, it is found that AO-PEG-Au NPs do not self-aggregate, whereas some aggregation phenomena occur in the case of the AO-TEG-Au NPs. The dimerisation constant obtained for the latter NP system is significantly high ($K_D = 6.3 \times 10^5$ $M^{-1}$) with respect to the values generally found for acridine dyes (for AHLB alone $K_D = 2.7 \times 10^3$ $M^{-1}$). This finding might be explained by taking into account that the presence of the nanoparticles produces a non-homogeneous distribution of the AO dye in the reaction medium that is locally concentrated on the NP.

For both nanoparticles it is found that, even if light absorption gives the main contribution to the observed spectral behavior, the light scattering (LS) component cannot be neglected. The LS contribution is proportional to $\lambda^{-n}$. It is found that for AO-TEG-Au NPs $n$ = 2.3–2.4 and for AO-PEG-Au NPs $n$ = 2.3–2.7, whereas for DNA/AO-TEG-Au NPs and DNA/AO-PEG-Au NPs absorbance titrations $n$ = 1.7–2.0 and $n$ = 1.5, respectively. The decrease of the $n$ value in the latter cases indicates that the size of the DNA/NPs systems is larger than that of the NPs alone.

The fluorescence characteristics of the two nanoparticles differ from each other. The fluorescence of both AO moieties attached to the NPs decreases considerably compared to the fluorescence intensity of free AHLB. However, although AO-TEG-Au NPs still moderately fluoresce, AO-PEG-Au NPs emit a negligible luminescence. This might be a consequence of some fluorescence quenching by the gold core which depends on the chain length of the AO linker.[13,37] Actually, previous studies showed that the efficiency of the fluorescence emission of the chromophore strongly depends on the metal surface–fluorophore distance ($d$).[38,39] It has been observed that strong quenching of fluorescence emission and a dramatic reduction of the lifetimes of the excited states occur when $d < 5$ nm, whereas these effects are not observed for $d >$ 10 nm.

As regards the interaction with natural DNA, the results show that this does take place. Indeed, it is suggested that the length of the ligand was adequately chosen to avoid steric hindrance effects by the TEG-SH tethers on the AO intercalating effectiveness. The discussion on the behavior of the nanoparticle/DNA systems is made easier by comparison with the AHLB/DNA system. The acridine derivatives are known to differently bind to DNA giving rise either to external or intercalated complexes, depending on the dye/DNA ratio.[16,35,40–43] Our data on the AHLB/DNA system also reveal the occurrence of two binding modes, the first one ($K_1 >$ $10^6$ $M^{-1}$) being likely related to external binding under dye excess conditions, the second one ($K_2 = 3.5 \times 10^4$ $M^{-1}$) corresponding to AO intercalation between DNA base pairs. Concerning the intercalative mode of binding, our $K$ values (Table 1) are in good agreement with literature data on the AO/DNA system under similar conditions.[16,44,45]

Absorbance titration results obtained for the AO-TEG-Au NPs/DNA system ($K = K_1 = 5.4 \times 10^6$ $M^{-1}$), compared with results obtained for the free AO derivative, suggest that AO-TEG-Au NPs are able to interact with DNA by external binding. On the other hand, the relatively low value of the binding constant

 

($K = K_2 = 3.8 \times 10^4$ $M^{-1}$) obtained from fluorescence data seems to indicate that some intercalation of the AO residue attached to the nanoparticle is also occurring.[45,46] Fluorescence data of the AO-PEG-Au NPs/DNA system show similarities with AO-TEG-Au NPs/DNA which suggest a dual mode of binding for the former system as well. The results show that the Acridine Orange residue, even if linked to a bulky substituent (nanoparticle), is able to intercalate into DNA, although the AO intercalation should be only partial. It was, indeed, found that the binding constant for intercalation into DNA of AO, under conditions similar to that used in present work, is close to $10^5$ $M^{-1}$,[45] whereas addition of substituents in the opposite position with respect to the aromatic nitrogen decreases the binding affinity ($K \leq 8 \times 10^4$ $M^{-1}$),[46] the latter finding being in agreement with the value obtained for AHLB intercalation into DNA (Table 2). If one reasonably supposes that a higher binding affinity reflects a deeper dye insertion, it can be suggested that dye penetration follows the order AO > AHLB > AO-Au NP.

Preliminary FACS flow cytometry tests indicate the AO-TEG-Au NPs are able to cross the cell membrane and are absorbed by the CHO cells at quite a low concentration. These results for the AO-TEG-Au NPs agree with previous findings that indicate that gold nanoparticles undergo endocytosis and that high NP uptake occurs under experimental conditions similar to those used in the present work (also important is likely to be the higher adhesion to cell membranes of cationic Au NPs with respect to anionic Au NPs).[47–49] Our results suggest that the absorption could occur on a picomolar scale with respect to the whole NP, opening the way for potential uses in cellular biology.

In summary, a multifunctional probe is able to bind to DNA with a characteristic photoresponse in both absorbance and emission and can cross the cellular membrane and be easily detected inside the cell.

## Acknowledgements

Prof Yitzhak Tor, Department of Chemistry & Biochemistry, University of California, San Diego, is kindly acknowledged for the research stage conducted by A. Schena at the UCSD laboratory and for helpful discussions. The authors thank Prof. B. H. Robinson for assistance in the editing of the English language.

## References

1 M. Han, X. Gao, J. Z. Su and S. Nie, *Nat. Biotechnol.*, 2001, **19**, 631–635.
2 M. E. Stewart, C. R. Anderton, L. B. Thompson, J. Maria, S. K. Gray, J. A. Rogers and R. G. Nuzzo, *Chem. Rev.*, 2008, **108**, 494–521.
3 A. K. Boal, F. Ilhan, J. E. Derouchey, T. Thurn-Albrecht, T. P. Russell and V. M. Rotello, *Nature*, 2000, **404**, 746–748.
4 S. K. Ghosh and T. Pal, *Chem. Rev.*, 2007, **107**, 4797–4862.
5 P. S. Ghosh, C.-K Kim, G. Han, N. S. Forbes and V. M. Rotello, *ACS Nano*, 2008, **2**, 2213–2218.
6 J. J. Storhoff and C. A. Mirkin, *Chem. Rev.*, 1999, **99**, 1849–1862.
7 D. A. Giljohann, D. S. Seferos, W. L. Daniel, M. D. Massich, P. C. Patel and C. A. Mirkin, *Angew. Chem., Int. Ed.*, 2010, **49**, 3280–3294.
8 A. Kanaras, F. S. Kamounah, K. Schaumburg, C. J. Kiely and M. Brust, *Chem. Commun.*, 2002, 2294–2295.
9 A. P. Alivisatos, K. P. Johnsson, X. Peng, T. E. Wilson, C. J. Loweth, M. Bruchez and P. J. Schultz, *Nature*, 1996, **382**, 609–611.
10 X. Li, J. Wang, L. Sun and Z. Wang, *Chem. Commun.*, 2010, **46**, 988–990.
11 S. Ribrioux, G. Kleymann, W. Haase, K. Heitmann, K. Ostermeier and H. J. Michel, *J. Histochem. Cytochem.*, 1996, **44**, 207–213.
12 U. H. F. Bunz and V. M. Rotello, *Angew. Chem., Int. Ed.*, 2010, **49**, 3268–3279.
13 G. Wang, J. I. Zhang and R. W. Murray, *Anal. Chem.*, 2002, **74**, 4320–4327.
14 B. H. Robinson, A. Löffler and G. Schwarz, *J. Chem. Soc., Faraday Trans. 1*, 1973, **69**, 56–69.
15 V. V. Tscharner and G. Schwarz, *Biophys. Struct. Mech.*, 1979, **5**, 75–90.
16 J. Kapuscinski and Z. Darzynkiewicz, *J. Biomol. Struct. Dyn.*, 1987, **5**, 127–143.
17 J. Sharma, R. Chhabra, C. S. Andersen, K. V. Gothelf, H. Yan and Y. Liu, *J. Am. Chem. Soc.*, 2008, **130**, 7820–7821.
18 G. Han, T. Mokari, C. Ajo-Franklin and B. E. Cohen, *J. Am. Chem. Soc.*, 2008, **130**, 15811–15813.
19 H. R. Mahler, B. Kline and B. D. Mehrotra, *J. Mol. Biol.*, 1964, **9**, 801–11.
20 P. Mulvaney, *Langmuir*, 1996, **12**, 788–800.
21 C. Courvoisier, M. J. Paret, J. Chantepie, J. Goré, G. Fournet and G. Quash, *Bioorg. Chem.*, 2006, **34**, 49–58.
22 E. Miethke and V. Zanker, *Z. Phys. Chem.*, 1958, **18**, 375–390.
23 Y. Kubo, S. Uchida, Y. Kenmochi and T. Okubo, *Tetrahedron Lett.*, 2005, **46**, 4369–4372.
24 L. A. Porter, D. Jr. Ji, S. L. Westcott, M. Graupe, R. S. Czernuszewicz, N. J. Halas and T. R. Lee, *Langmuir*, 1998, **14**, 7378–7386.
25 H. P. Klug and L. E. Alexander, in *X-ray Diffraction Procedures: for Polycrystalline and Amorphous Materials*, 2nd edn, J. Wiley and Sons Inc., New York, 1974.
26 A. Henglein and M. Giersig, *J. Phys. Chem. B*, 1999, **103**, 9533–9539.
27 U. Hotje, C. Rose and M. Binnewies, *Solid State Sci.*, 2003, **5**, 1259–1262.
28 A. I. Frenkel, S. Nemzer, I. Pister, L. Soussan and T. Harris, *J. Chem. Phys.*, 2005, **123**, 184701.
29 T. Shimizu, T. Teranishi, S. Hasegawa and M. Miyake, *J. Phys. Chem. B*, 2003, **107**, 2719–2724.
30 S. J. Leach and H. A. Scheraga, *J. Am. Chem. Soc.*, 1960, **82**, 4790–4792.
31 B. E. Bowler, K. J. Ahmed, W. I. Sundquist, L. S. Hollis, E. E. Whang and S. J. Lippard, *J. Am. Chem. Soc.*, 1989, **111**, 1299–1306.
32 T. Biver, B. García, J. M. Leal, F. Secco and E. Turriani, *Phys. Chem. Chem. Phys.*, 2010, **12**, 13309–13317.
33 G. G. Hammes and C. D. Hubbard, *J. Phys. Chem.*, 1966, **70**, 2889–2895.
34 A. D. James and B. H. Robinson, *Adv. Mol. Relax. Processes*, 1976, **8**, 287–304.
35 M. B. Lyles and I. L. Cameron, *Biophys. Chem.*, 2002, **96**, 53–76.
36 E. Fredericq and C. Houssier, *Biopolymers*, 1972, **11**, 2281–2308.
37 K. George Thomas and P. V. Kamat, *Acc. Chem. Res.*, 2003, **36**, 888–898.
38 U. H. F. Bunz and V. M. Rotello, *Angew. Chem., Int. Ed.*, 2010, **49**, 3268–3279.
39 K. Aslan and V. H. Perez-Luna, *J. Fluoresc.*, 2004, **14**, 401–405.
40 C. Ciatto, M. L. D'Amico, G. Natile, F. Secco and M. Venturini, *Biophys. J.*, 1999, **77**, 2717–2724.
41 T. Biver, C. Ciatto, F. Secco and M. Venturini, *Arch. Biochem. Biophys.*, 2006, **452**, 93–101.
42 B. García, J. M. Leal, R. Ruiz, T. Biver, F. Secco and M. Venturini, *J. Phys. Chem. B*, 2010, **114**, 8555–8564.
43 C. Bazzicalupi, A. Bencini, A. Bianchi, T. Biver, A. Boggioni, S. Bonacchi, A. Danesi, C. Giorgi, P. Gratteri, A. Marchal Ingraín, F. Secco, C. Sissi, B. Valtancoli and M. Venturini, *Chem.–Eur. J.*, 2008, **14**, 184–196.
44 S. Nafisi, A. A. Saboury, N. Keramat, J. Neault and H. Tajmir-Riahi, *J. Mol. Struct.*, 2007, **827**, 35–43.
45 W. Muller and D. M. Crothers, *Eur. J. Biochem.*, 1975, **54**, 267–277.
46 W. Muller, H. Bunemann and N. Dattagupta, *Eur. J. Biochem.*, 1975, **54**, 279–291.
47 K. Song, P. Xu, Y. Meng, J. Chen, X. Yang, W. Roa, B. Kong and J. Xing, *IEEE/NIH Life Sci. Syst. Appl. Workshop*, 2009, 33–35.
48 K. Y. Win and S.-S. Feng, *Biomaterials*, 2005, **26**, 2713–2722.
49 J. Lin, H. Zhang, Z. Chen and Y. Zheng, *ACS Nano*, 2010, **4**, 5421–5429.